Alan H. Wilman, PhD • Stephen J. Riederer, PhD • Bernard F. King, MD • Josef P. Debbins, MSEE
Phillip J. Rossman, MS • Richard L. Ehman, MD

Fluoroscopically Triggered Contrast-enhanced Three-dimensional MR Angiography with Elliptical Centric View Order: Application to the Renal Arteries[1]

PURPOSE: To determine the reliability of obtaining arterial-phase, contrast-material–enhanced three-dimensional (3D) magnetic resonance (MR) angiograms of the renal arteries by using a technique that combines two-dimensional real-time MR fluoroscopy and a 3D MR angiographic acquisition with elliptical centric view order.

MATERIALS AND METHODS: Twenty-five consecutive patients suspected of having renal artery disease were evaluated with the fluoroscopically triggered technique by using a mean dose of 0.18 mmol/kg gadoteridol. Left renal vein suppression, inferior vena cava suppression, motion artifact, and image quality for depiction of the renal arteries were each evaluated on a five-point scale (1 = best). The findings were compared with those of another 25 consecutive patients who underwent conventional gadolinium-enhanced 3D MR angiography.

RESULTS: The fluoroscopically triggered technique produced 4.6 times less left renal vein enhancement than did the conventional method (*P* < .01). With the fluoroscopically triggered technique, visualization of the renal arteries was adequate for diagnosis in 24 patients (96%) and the overall result (score of 1–3 for all criteria) was of good quality in 22 patients (88%).

CONCLUSION: With this fluoroscopically triggered MR angiographic technique, high-quality, arterial phase, relatively motion immune angiograms can be routinely obtained.

THE success of gadolinium-enhanced magnetic resonance (MR) angiography (1,2) is dependent on delivery of the gadolinium chelate through the vascular system to the site of interest. It is well accepted that low-order phase-encoding views dominate image contrast (3); thus, to obtain first-pass arterial-phase images, the central k-space views should ideally be acquired at peak arterial enhancement (4). For two-dimensional (2D) imaging of a single section, this is not difficult to achieve due to the intrinsic high temporal resolution (5–7). However, for three-dimensional (3D) imaging with acquisition times of several tens of seconds, the issue of bolus timing is very important, especially since bolus transit times can vary substantially between patients (8,9). The initial work in 3D gadolinium-enhanced MR angiography used continuous infusion and an imaging time much longer than the variability in transit time, making the timing issue moot (1,10). This approach, however, was susceptible to both respiratory motion and venous contamination, and also suffered from continual dilution of the contrast material due to the lengthened acquisition time. More recent, many 3D studies were performed with use of rapid injection and a rapid acquisition protocol (8,11–14). This approach has the potential to reduce re-

spiratory artifact, venous contamination, and the required dosage of contrast material. With this approach, however, timing the acquisition with the arrival of the bolus of contrast material then becomes extremely important (4,8,11,15).

A number of methods for timing the data acquisition with the arrival of the bolus of contrast material to produce 3D arterial-phase images have already been presented. These include (*a*) estimation of the time of arrival, (*b*) injection of a small amount of contrast material in a test dose to establish timing (16), (*c*) partial k-space updating with increased time resolution (17), and (*d*) line scanning before 3D triggering (18). These methods have all been successful to varying degrees. Nevertheless, each method has a potential drawback as discussed below. For method *a*, the time-to-enhancement variability between patients can be problematic. For method *b*, the test dose causes increased vascular enhancement and causes accumulation of contrast material in the renal pelvis, neither of which is generally desirable. Furthermore this method requires that the cardiac output remain unchanged between the test acquisition and the actual 3D acquisition, which may not always be true. For method *c*, the repetitive sampling of k space ensures an arterial-phase image,

Figure 1. Schematic diagram of possible contrast-enhanced 3D MR angiographic (*MRA*) acquisitions. In *a*, a typical contrast curve of arterial and venous enhancement is shown. In *b*, the fluoroscopically triggered pulse sequence is shown. This sequence is initiated just before injection of contrast material, and continuous fluoroscopic imaging occurs at an interactively prescribed location. Once the contrast agent is detected, the 3D image with centric phase-encoding order is triggered. For breath-hold studies, breath holding is coached just before triggering. In *c* and *d*, the two possible timings for the conventional sequential phase-encoding order are shown (see text for details). In *e*, the elliptical spiral and sequential view orders are illustrated for an 8 × 8 phase-encoding matrix. During every repetition of a 3DFT acquisition, the signal collected corresponds to one of the points shown, with sampling along an axis corresponding to the frequency direction, k_x, coming out of the plane of the plot. Note that the shaded central views are played out first with the elliptical centric approach. T_{ell} and T_{seq} = time to sample the central views in the elliptical centric method and the sequential method, respectively.

but within a given breath-hold length, the total k-space coverage must be limited to allow for sufficient repetitive view sampling. Finally, although method *d* monitors the bolus arrival in real time, this approach does not give an image-based view of the arrival of contrast material and requires the setting of an automatic threshold level that may not account for variability in the degrees of contrast enhancement between patients.

Thus, we developed a technique for direct monitoring of arrival of the contrast material in a sequence of real-time "MR fluoroscopic" images with means for immediate triggering of a 3D MR angiographic sequence. This technique overcomes all the aforementioned disadvantages by making use of direct monitoring rather than prediction, by maximizing the spatial resolution for a given breath hold, by providing a temporal series of 2D images that illustrates the dynamics of the arrival of contrast material, and by allowing for manual triggering of the 3D acquisition by the operator.

Accurate timing alone is not sufficient to achieve the ideal angiographic result in which the arterial system has high signal intensity and the venous system has no signal. To achieve this, the 3D MR angiographic acquisition is ideally performed in a manner to maximize immunity of the technique to contrast enhancement of the venous vasculature. The question of the determination of the best method for sampling k space has already been raised (8). To this end, we recently developed an "elliptical centric" phase-encoding
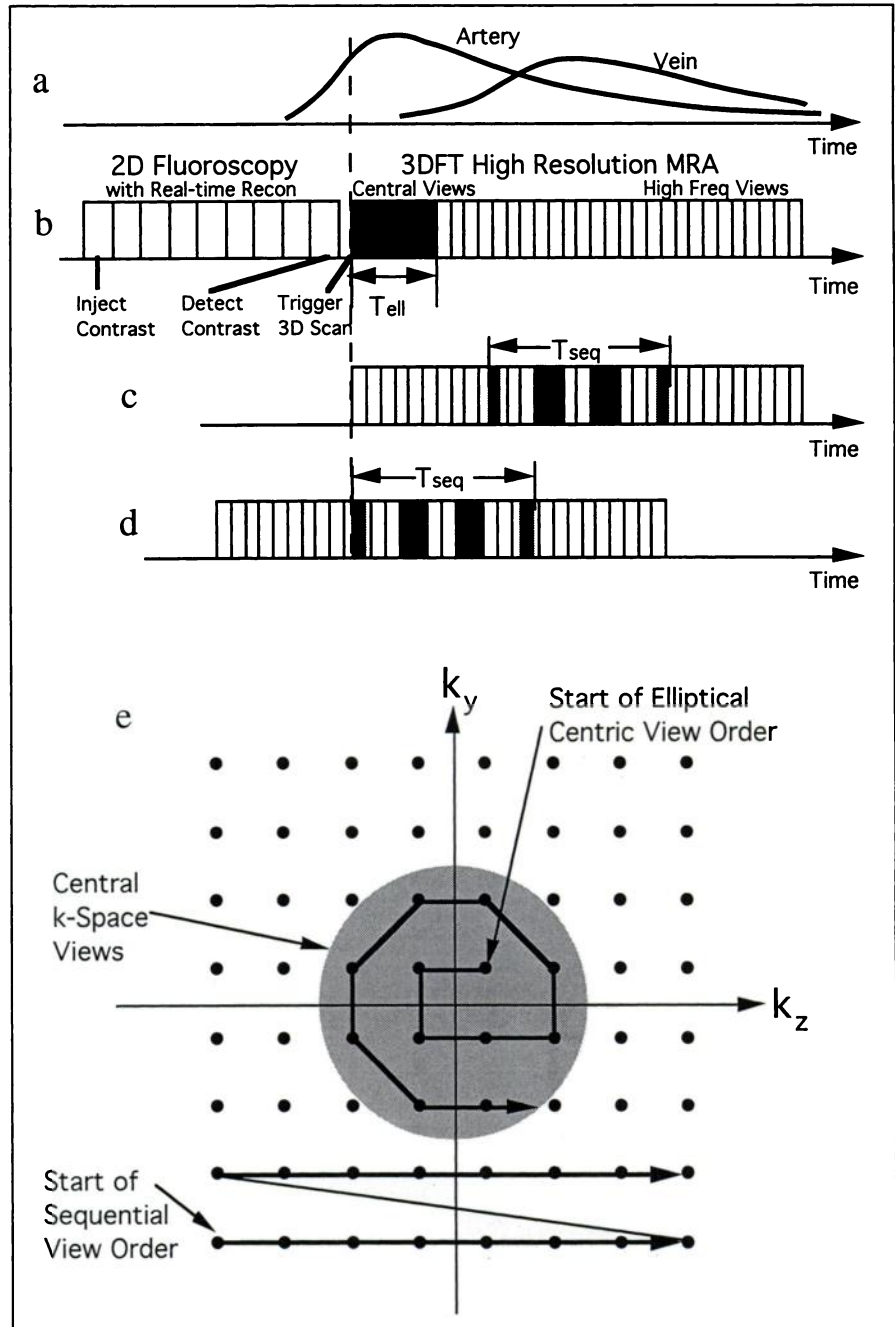
order for 3D Fourier transform (FT) gradient-echo imaging that has been shown in studies in phantoms and volunteers to provide improved immunity to venous enhancement and to motion compared with many other view orders for 3DFT imaging (19–21).

The purpose of this study was to apply the technique of fluoroscopically triggered contrast material–enhanced 3DFT acquisition in conjunction with the elliptical centric view order in a set of consecutive patients referred for MR imaging evaluation of the renal arteries. We compared the results of this technique with those in a similar set of consecutive patients who underwent conventional con-

trast-enhanced 3D MR angiographic examination.

MATERIALS AND METHODS

Overview of Fluoroscopic Technique

A timing diagram of contrast-enhanced 3D MR angiography with fluoroscopic triggering and centric view order is shown in Figure 1 parts *a* and *b*. For purposes of discussion, suppose that the origins of the renal arteries are to be imaged by using a 25-second 3DFT MR angiographic acquisition. Before the actual injection of contrast material, all imaging parameters for the 3D sequence are determined and loaded into the pulse sequence controller, and the 3D sequence is thus ready for immediate

Table 1
Evaluation Criteria for Qualitative Evaluation of Contrast-enhanced 3D MR Angiograms

Score	Left Renal Vein Suppression	Inferior Vena Cava Suppression	Motion Artifact	Image Quality for Depiction of Renal Arteries
1	No signal from left renal vein	No signal from inferior vena cava	No visible artifact	Excellent
2	Barely visible signal intensity	Barely visible signal intensity	Minimal artifact	More than adequate for diagnosis
3	Noticeable signal intensity but less than that of the left renal artery	Noticeable signal intensity but less than that of the aorta	Moderate artifact without serious impairment of vessel visualization	Adequate for diagnosis
4	Signal intensity equal to that of the left renal artery	Signal intensity equal to that of the aorta	Moderate artifact with serious impairment of vessel visualization	Less than adequate for diagnosis
5	Signal intensity greater than that of the left renal artery	Signal intensity greater than that of the aorta	Severe artifact, nondiagnostic	No visualization

Table 2
Blood Vessel Signal Intensity Measurements (Normalized to Aortic Noise)

Blood Vessel	Conventional 3D MR Angiography		Fluoroscopically Triggered 3D MR Angiography	
	Before Injection	During Injection	Before Injection	During Injection
Aorta	1.8 ± 1.0	24.5 ± 11.7	2.2 ± 1.4	22.4 ± 10.2
Inferior vena cava	1.6 ± 1.1	6.8 ± 6.0	2.1 ± 1.5	3.2 ± 2.4
Left renal artery	2.1 ± 1.8	19.5 ± 9.1	2.2 ± 1.3	18.2 ± 7.2
Left renal vein	1.8 ± 0.9	14.4 ± 11.1	1.9 ± 0.9	5.2 ± 4.1
Vena cava–to–aorta enhancement ratio	0.26 ± 0.28		0.06 ± 0.05	
Left renal vein–to–artery enhancement ratio	0.88 ± 0.86		0.19 ± 0.18	

execution. Next, a plane is selected to be monitored by the real-time 2DFT fluoroscopic sequence. For the current study, this plane was usually chosen to be a 10-mm-thick sagittal section that contained the thoracic and abdominal aorta as best as possible. With both the 3D and fluoroscopic sequences loaded, execution of the actual contrast-enhanced procedure can commence. As shown in part b, just before administration of the contrast agent the fluoroscopic sequence is initiated and applied continuously. While the contrast material is en route to the targeted vasculature, the operator monitors the aorta by viewing the fluoroscopic images, each of which is reconstructed within several hundred milliseconds after acquisition. On seeing the contrast material in the aorta, the operator can optionally direct the patient to hold his or her breath and then immediately trigger the 3DFT MR angiographic sequence. In this way, 3D imaging is initiated while the contrast material is entering the targeted arterial anatomy, at the outset of a breath hold, and with central k-space views acquired during maximal arterial enhancement.

MR Angiographic Sequence: Elliptical Centric View Order

The 3D MR angiographic portion of the technique makes use of the elliptical centric view order (20–22), which, as shown in

Figure 1, differs greatly from the conventional sequential view order. In parts b–d, the temporal playouts of the two orders are compared. The 3D playout in k space is shown in part e, where the two axes shown correspond to the two phase-encoding directions, k_y and k_z. The shaded area represents the "central" views, which correspond to the lowest spatial frequencies and dominate image contrast. For the case of a sequential acquisition of k-space views, the first repetition samples the lowest leftmost point, the next repetition samples the point immediately to the right, and this continues until the lowest row is completely sampled. The next higher row is then sampled similarly, and this process repeats until all desired points are sampled. Conversely, for the elliptical centric view order, the readout during the first repetition of the acquisition starts with one of the k-space points closest to the origin, and in subsequent repetitions points are sampled at progressively larger radii in this k space. In this manner, the central views are sampled earliest in the acquisition, and those points at larger k_y and k_z distances (which sample higher spatial frequencies) are sampled later.

The spacing between the sampled points in the k-space plots of Figure 1 part e is dictated by the fields of view (FOVs) along the y and z directions. Here, these FOVs are assumed to be equal, and consequently, the spacings are the same along k_y and k_z.

For the general case these FOVs are different, resulting in different spacings along k_y and k_z, which requires a modification of the sampling order to maintain a circular trajectory in k space. Often, the inverse FOV spacing is discounted when plotting k-space indexes, and the points are plotted on a grid with equal spacing. In this case, the circular trajectory of part e becomes an elliptical one when the FOVs differ; hence, the name "elliptical centric."

The inherent ability of the elliptical centric view order to provide improved immunity to venous enhancement can perhaps be understood by again considering Figure 1 parts a–d. Part a demonstrates hypothetical curves that show the behavior over time of contrast enhancement in the arteries followed several seconds later by enhancement in the veins, the specific delay dependent on the vasculature under consideration. Part b, after 3D triggering, shows the 3D acquisition corresponding to the elliptical centric view order of part e. Each temporal division represents the acquisition of two points of the plot in part e. As shown, the 12 points of the central region of part e are sampled at the shaded outset of the acquisition in part b, here during peak arterial contrast enhancement and before any venous contrast enhancement.

The sequential view order in part c differs from the elliptical centric case in part b in two important respects. First, the central views are acquired much later during data acquisition, centered halfway through. For the case shown in Figure 1 part c, these views would undesirably be sampled well after peak arterial enhancement and during peak venous enhancement. The central views of the sequential acquisition could be matched to peak arterial enhancement as shown in part d, but in that case a number of the initial high k-space views would be acquired before the contrast material arrives in the targeted vasculature. A second important difference between sequential and elliptical centric view orders is the time it takes to sample the central views. Ideally, one wishes to sample these views in the shortest time possible at peak arterial enhancement, which will minimize the likelihood of venous enhancement. The elliptical centric method achieves this goal;

however, the sequential approach plays out the central views over a substantially longer time period (compare T_{seq} in part d with T_{ell} in part b).

To summarize, the elliptical centric view order samples the central views at the outset of the acquisition and acquires the central views in the shortest time possible. The desirability to initiate a 3DFT acquisition with the elliptical view order at the onset of arterial enhancement provides the motivation for a means for accurate triggering.

MR Fluoroscopy Sequence

The fluoroscopic portion of the integrated pulse sequence was first used to determine the viewing plane to monitor the arrival of contrast material. This was accomplished in a simple and rapid manner by using a cursor-defined off-isocenter rotation under interactive fluoroscopic control (23). Specifically, beginning with an axial view of the abdomen nominally at the level of the renal artery origins, a cursor was placed on the image at the center of the aorta, and the image plane was then rotated 90° about the cursor into a sagittal view at the prescribed cursor location. If necessary, further small-angle rotations and adjustments in FOV or section thickness were made to improve the length and quality of aortic visualization. Typically, the time for selecting the aortic viewing plane was about 1 minute. Once the viewing plane was established, the patient was coached to hold his or her breath and a test 3D image set was obtained without administration of contrast material to ensure accurate selection of the 3D volume. Next, the sequence as shown in Figure 1 part b was performed.

The fluoroscopic image parameters were chosen to produce dynamic 2D images with high spatial resolution under the constraint of keeping the image update rate no slower than about one per second. This temporal resolution was considered marginally sufficient for observing the arrival of contrast material into the abdominal aorta. Thus, the typical fluoroscopic scanning parameters included the following: 13–15/8 (repetition time [TR] msec/echo time msec), 30° flip angle, 10-mm section thickness, 256 (x) × 96 (y) matrix, ±16-kHz receiver bandwidth, and first-order gradient moment nulling in the section-select and frequency directions. The relatively long echo time of 8 msec was necessary to allow for a full echo acquisition at a relatively low bandwidth, for the use of gradient moment nulling, and for oblique imaging with an FOV as small as 200 mm. The use of gradient moment nulling reduced flow dephasing effects; this was particularly valuable in the initial scouting process before the arrival of contrast material. The flip angle was chosen to be large enough to saturate in-plane flow, thus allowing for substantial contrast material enhancement but also to be sufficiently small such that the images obtained before the arrival of contrast material were not completely saturated. As mentioned above, the fluoro-
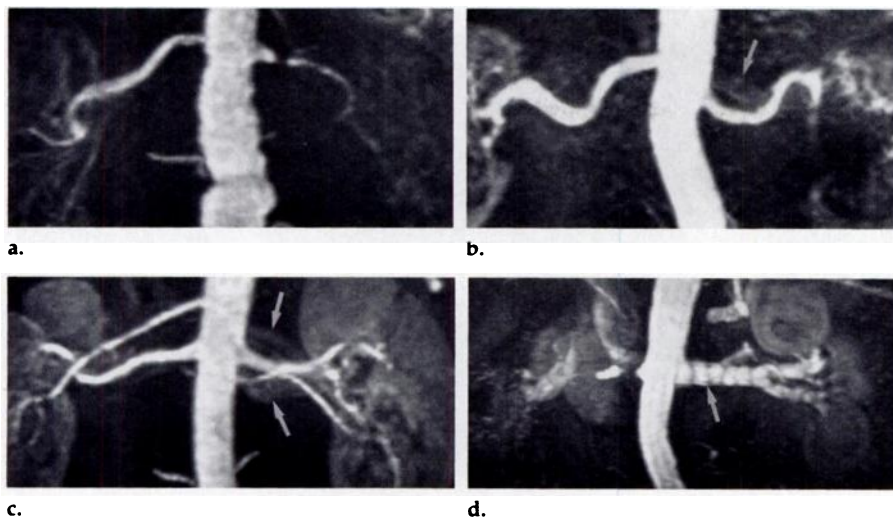
scopic imaging rate was approximately one per second (96 views × 13 msec). The 96 views represented three-quarter partial Fourier sampling of 128 views, with the latter quarter zero filled; further symmetric zero filling to 256 points was performed before reconstruction. The reconstruction time was ~500 msec for the 256 × 256 matrix when using a four-coil phased array and a "sum of the squares" reconstruction (24).

Instrumentation for Fluoroscopic Triggering

Actual implementation of fluoroscopic triggering of the 3D angiographic sequence requires instrumentation capable of several distinct functions. These include (a) the ability to rapidly switch from one pulse sequence to another, (b) the ability to reconstruct the 2DFT fluoroscopic images very quickly, and (c) the means for

allowing the operator to manually trigger the 3DFT sequence. These functions were achieved by making use of an "MR fluoroscopy" apparatus (25), which has recently been described in detail (26). This real-time reconstruction system has been interfaced to a standard whole-body 1.5-T MR imaging unit (Signa; GE Medical Systems, Milwaukee, Wis).

The first function above, sequence switching, is provided by copying both the fluoroscopic and 3D pulse sequences into the pulse controller memory of the MR imaging unit. At the outset of contrast-enhanced imaging, a logic variable is set to "true," and after each 13-msec repetition of the fluoroscopic sequence the variable is evaluated. If "true," the fluoroscopic sequence is repeated; if "false," the sequence controller switches to the 3D sequence. Once triggered, there is an additional 10-msec latency until execution of the 3D se-

Table 3

Comparison of Conventional and Fluoroscopically Triggered 3D Contrast-enhanced MR Angiography

Category*	Conventional	Triggered	P Value
Left renal vein suppression	2.8 ± 1.2	1.4 ± 0.7	<.0001
IVC suppression distal to renal veins	2.0 ± 0.9	1.2 ± 0.4	<.001
IVC suppression below renal veins	1.3 ± 0.7	1.0 ± 0.0	<.015
Motion artifact	2.0 ± 1.3	1.7 ± 0.8	<.15
Image quality for depiction of renal arteries	2.3 ± 1.2	1.5 ± 0.9	<.02

Note.—Data are presented as the mean ± standard deviation. Images from all 50 patients were evaluated on a five-point scale (1 = best, 5 = worst) as detailed in Table 1.
* IVC = inferior vena cava.
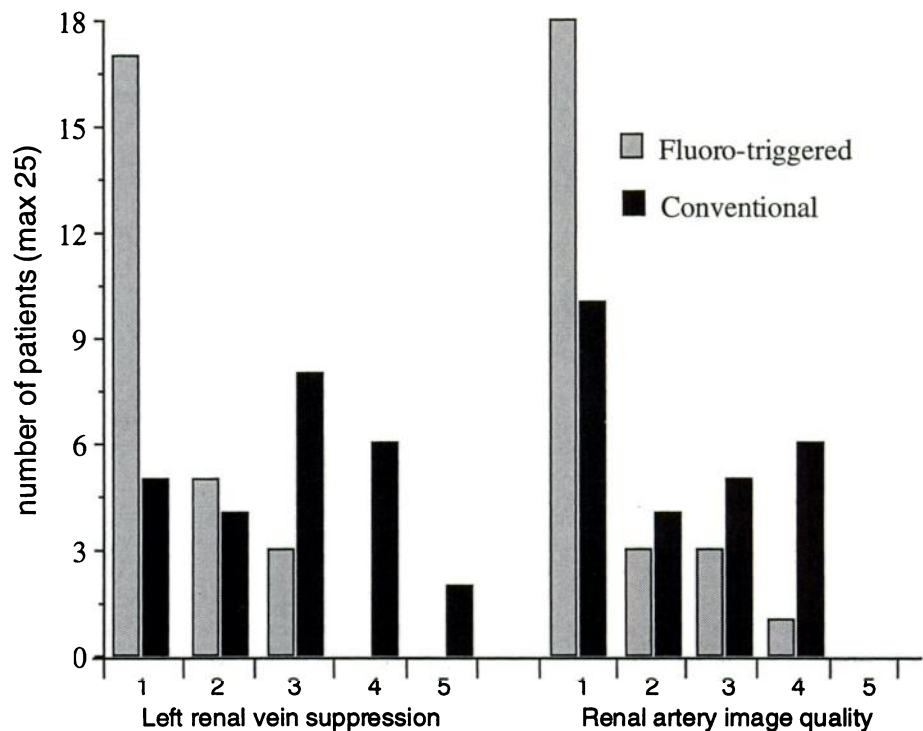
Figure 2. Illustration of the distribution of patients in the evaluation of left renal vein suppression and renal artery image quality. The improvement with the fluoroscopically triggered sequence was statistically significant for both the left renal vein suppression and the renal artery categories. In the latter category, the only grade 4 score in the fluoroscopically triggered acquisitions was due to a verbal communication error.

Figure 3. Coronal MIP images from the 3D data sets illustrate varying degrees of left renal vein suppression. **(a)** No renal vein was evident (grade 1). **(b)** Left renal vein (arrow) is barely visible (grade 2). **(c)** Left renal veins (arrows) are noticeable but less so than the renal artery (grade 3). **(d)** Left renal vein signal intensity (arrow) is equal to that of the renal artery (grade 4). The images in a–c are from fluoroscopically triggered, elliptical centric phase-encoding order data sets. The image in d is from a nontriggered, sequential acquisition data set. In terms of motion artifact, **a** and **b** received a grade of 2 due to minimal artifact, while **c** and **d** had no visible artifact (grade 1).

quence. The second function, high-speed reconstruction, is performed as discussed above with the array processor integral to the instrumentation discussed by Debbins et al (26). The third function, operator intervention, is provided by a direct serial interface from the host computer of the MR fluoroscopy system to the pulse sequence controller. By clicking a mouse corresponding to a "trigger" button on the display screen, the operator causes the logic variable described above to change from true to false. The total delay from acquisition of data for the contrast-filled fluoroscopic image until initiation of the 3DFT MR angiographic sequence is thus 523 msec (500 + 13 + 10) plus the response time of the operator.

Patient Studies

The fluoroscopically triggered breath-hold contrast-enhanced 3D pulse sequence with elliptical centric view order was tested on 25 consecutive patients who had been referred for MR examination of the renal arteries. There were 16 male and nine female patients with a mean age of 64 years ± 17 (age range, 17–78 years) and mean weight of 84 kg ± 21. Their serum creatinine levels ranged from 0.7 to 2.5 mg/dL (60–220 μmol/L) with a mean of 1.5 mg/dL ± 0.7 (130 μmol/L). Each patient received a 30-mL dose (mean dose, 0.18 mmol/kg ± 0.05) of gadoteridol (Prohance; Bracco Diagnostics, Princeton, NJ) by hand injection into a forearm vein with an 18-gauge angiographic catheter at a rate of 3–5 mL/sec. This was followed by a saline flush of 20 mL. The 3D MR angiographic portion of the integrated pulse sequence was prescribed to image the renal arteries and abdominal aorta in the coronal plane. The 3DFT MR angiographic acquisition used radio-frequency spoiling, re-

winding of both phase-encoding gradients, 7.2/1.3, 45° flip angle, matrix size of 256 (x) × 128 (y) × 32 (z) with 1.5–2.0-mm section thickness, three-quarter or full FOV in the y direction, ±32-kHz receiver bandwidth, and acquisition time of 24–32 seconds. Either a dual-element "license plate" coil (GE Medical Systems) or a four-element phased-array coil (27) was used. Each patient was instructed to hold his or her breath at end-inspiration immediately before triggering the 3D acquisition.

The results from the fluoroscopically triggered sequence were compared with those in a similar population of 25 consecutive patients (14 men, 11 women; mean age, 64 years ± 11; age range, 35–79 years; mean weight, 78 kg ± 19; serum creatinine level: mean, 1.6 mg/dL ± 0.7 [140 μmol/L]; range, 0.7–3.2 mg/dL [60–280 μmol/L]). The same 30-mL dose (mean dose, 0.20 mmol/kg ± 0.5) and injection scheme were used. These patients had undergone gadolinium-enhanced 3D MR angiography during the 4 months prior to the availability of the fluoroscopically triggered sequence. In these patients, 3D imaging commenced approximately 12–15 seconds after the injection was begun, similar to the technique used by Leung et al (14). This standard 3D technique made use of sequential view order and was typically performed with the following parameters: 45° flip angle, ±32-kHz bandwidth, three-quarter phase FOV, 512 × 128 × 32 matrix with 10.5/1.8 or 512 × 160 × 16 matrix with 12.7/2.4. A dual-element license plate receive coil was used, and the breath-hold length was 20–32 seconds.

Evaluation

The fluoroscopically triggered technique was evaluated in two ways. First, the fluo-

roscopic portion of the procedure was evaluated by determining if it was possible to trigger the 3D MR angiographic sequence on the basis of visualization of the contrast agent on the fluoroscopic image sequence. Second, the fluoroscopic image sequence for each patient was used to determine the actual time delay from start of injection to arrival of contrast material in the abdominal aorta and the degree of signal enhancement. The latter was defined as the ratio of signal intensity measurements on the fluoroscopic images obtained just before triggering of the 3D image to those obtained just before injection. The signal intensity was the average value from a ~1-cm² region of interest within the aorta at the nominal level of the renal arteries.

Qualitative and quantitative evaluations were also performed on the 3D MR angiograms obtained with the fluoroscopically triggered technique with elliptical centric view order and on those obtained with sequential view order with no triggering. Five criteria were chosen for the qualitative evaluation of the 3D MR angiograms by using a five-point scale (Table 1). Evaluations were done on an examination-by-examination basis, with consideration of both hard-copy films and video displays of the maximum intensity projection (MIP) images and individual partitions. Each grade represented the consensus of the three senior authors (A.H.W., S.J.R., B.F.K.). To assess the degree of venous suppression, the signal intensity of the left renal vein relative to that of the left renal artery was graded. Similarly, the degree of contrast enhancement in the inferior vena cava proximal and distal to the confluence with the right renal vein was also evaluated. The degree of apparent motion artifact was also assessed. Finally, the overall quality of each MR angiographic examination in terms of degree of portrayal of the main renal arteries was assessed. For each comparison, the mean and standard deviation of each group were computed, and the Wilcoxon rank-sum test was performed to determine statistical significance ($P < .05$) (28). For the quantitative evaluation, signal intensity measurements were obtained from the 3D MR angiographic source images at the following four locations: the aorta at the level of the renal arteries, the inferior vena cava distal to the confluence with the right renal vein, the main left renal artery, and the main left renal vein. These measurements were normalized to the aortic noise as reported by Prince (2). The venous-to-arterial enhancement ratio, V/A, was computed by taking the differences in signal intensity, SI, between the acquisitions obtained during, SI_d, and those obtained before, SI_b, passage of contrast material and is expressed by the following equation: $V/A = (VSI_d - VSI_b)/(ASI_d - ASI_b)$. Ideally, this enhancement ratio would be 0.

RESULTS

The results from the comparison of the fluoroscopically triggered 3D MR

a. **b.** **c.**
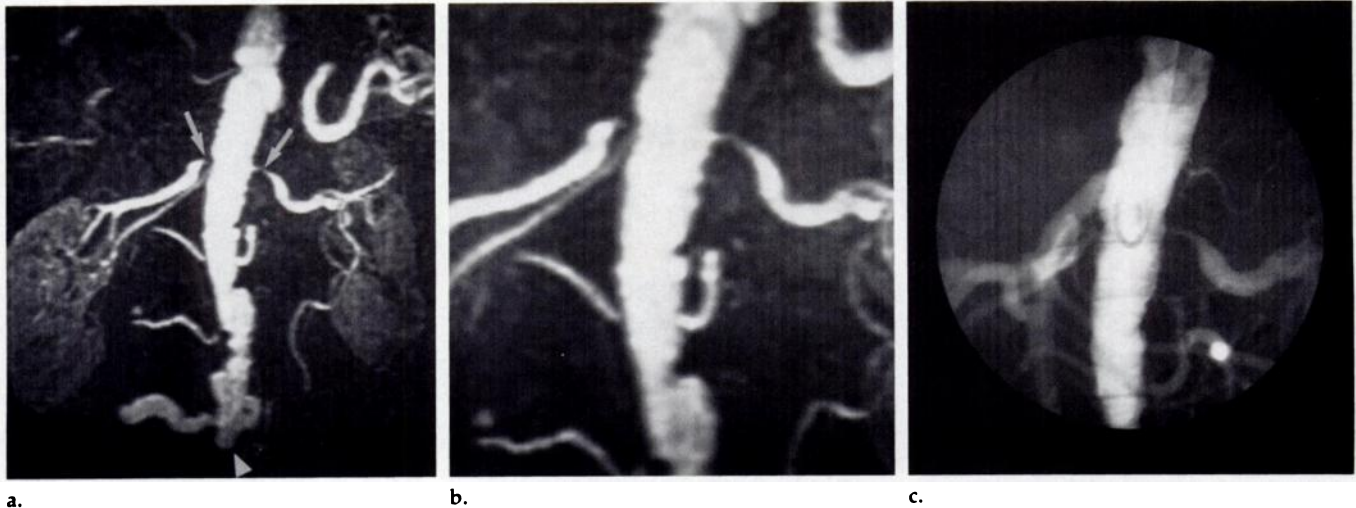
Figure 4. Angiograms in a patient with bilateral renal artery stenoses and a distal aortic occlusion with collateral flow being supplied by the lumbar arteries. **(a)** Coronal MIP image of 12 sections illustrates the bilateral renal artery stenoses (arrows) and distal aortic occlusion (arrowhead). **(b)** Renal artery portion has been enlarged for comparison with the x-ray angiogram **(c)** for which a pigtail catheter was used. The MR matrix size was 256 (x) × 128 (y) × 32 (z), with 1.5-mm resolution in z. The acquisition time was 34 seconds and the dual-element license plate coil was used.

angiographic sequence with the standard 3D MR angiographic technique are summarized in Tables 2 and 3. The signal intensity measurements of Table 2 show that the fluoroscopically triggered technique produced significantly less venous enhancement for the 3D acquisition during contrast administration. In particular, the venous-to-arterial enhancement ratios differed by a factor of greater than 4 for both the inferior vena cava–to–aorta ratio ($P < .01$) and the left renal vein–to–left renal artery ratio ($P < .001$). The results for the graded evaluation are shown in Table 3, and the corresponding distributions for two individual categories, left renal vein suppression and renal artery image quality, are shown in Figure 2. From Table 3 and Figure 2, it is again clear that the fluoroscopically triggered technique with elliptical centric view order was significantly superior for renal vein suppression. In all of the fluoroscopically triggered cases, the renal vein suppression was sufficiently low such that the main renal arteries could be easily identified on a coronal MIP image of the complete imaging volume. To aid in interpreting the numeric grades presented here, Figure 3 illustrates examples of different grades of left renal vein suppression. These images are coronal MIP images of the renal arteries and veins and represent the first four levels of the left renal vein evaluation scale.

The fluoroscopically triggered method also received a better grading for renal artery quality, and the degree of improvement over the conventional technique was statistically significant

Figure 5. Contrast-enhanced 3D MR angiograms from a fluoroscopically triggered data set with 1.5-mm section-select resolution. By making use of fine resolution in the section-select direction, the vessels may be well visualized from multiple angles. **(a)** Coronal MIP image of the full data set illustrates the left renal artery stenosis (arrow) and moderate atherosclerotic disease of the aorta. **(b)** Selective axial MIP image that includes all of the sections clearly shows the stenosis (arrow) in another orthogonal projection.

(Table 3). In addition, from the distribution in Figure 2, with use of the fluoroscopically triggered sequence, the renal arteries were well visualized in 24 (95%) of the 25 consecutive patients. On the basis of the MR examinations only, it was determined that of the 25 patients in the fluoroscopically triggered group, 15 patients had greater than 60% renal artery stenosis with five of these patients exhibiting bilateral stenoses; one case was indeterminate. The single case of poor visualization (grade 4) was due to improper verbal communication, which led to premature triggering of the 3D image. Of the 25 patients in the conventional technique group, seven patients had greater than 60% stenosis with one having bilateral stenoses, and four cases were indeterminate due to poor quality.

In 18 (72%) of the 25 fluoroscopically triggered cases, the overall result was considered high quality, defined as a score of 1 or 2 for all five evaluation criteria. In 22 (88%) of these 25 cases, the result was considered good quality, defined as a score of 1, 2, or 3 for all criteria. In comparison, for the patients in the conventional method

a.

b.
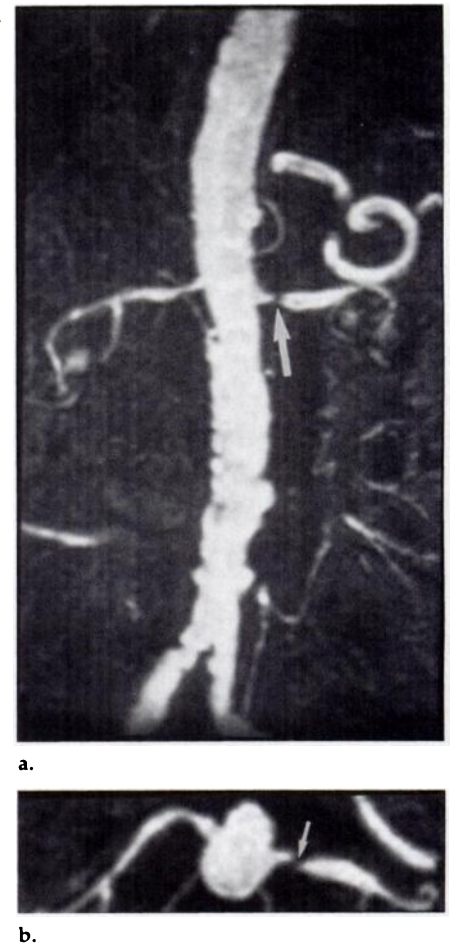
group, the respective frequencies were six (24%) and 14 (56%) of 25 patients.

The superior image quality of the 3D data sets from the fluoroscopically triggered pulse sequence was particularly helpful in several difficult patients. In Figure 4a, the selective coronal MIP

a.
b.
c.
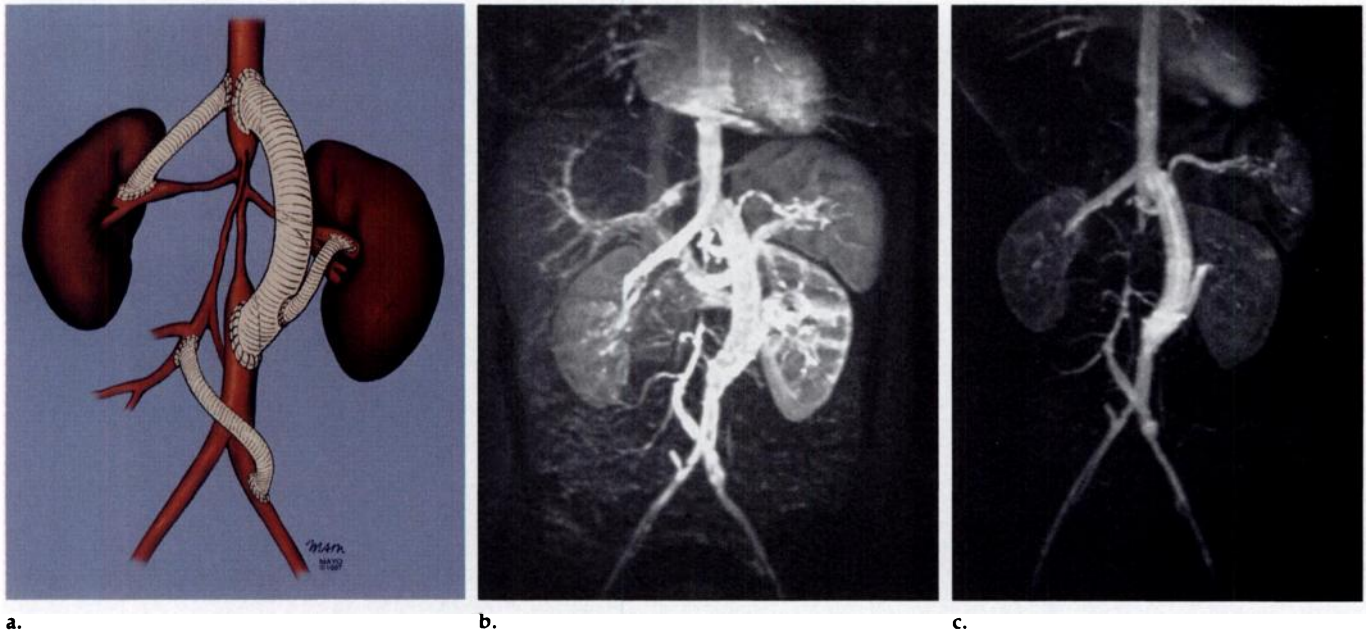
Figure 6. Takayasu arteritis in a patient with multiple grafts to the aorta. **(a)** Sketch of this patient's specific anatomic features shows the grafts in beige. **(b, c)** Three-dimensional MR angiographic MIP images from this patient's complete data set were obtained by using two different techniques. **(b)** MIP image obtained with the conventional technique that uses sequential phase encoding and estimation of the bolus timing. The 3D acquisition was 32 seconds in duration and was begun 4 seconds after administration of contrast material. The combination of rapid circulation time and sequential phase encoding caused substantial venous enhancement. **(c)** Follow-up MIP image obtained 6 months later with use of the fluoroscopically triggered pulse sequence shows minimal venous signal intensity. The discontinuity in the lumen of the proximal superior mesenteric artery arises from the inflammation and fibrosis of the Takayasu disease. The lumen of the distal superior mesenteric artery is patent with blood supply via a graft from the left iliac artery.

image illustrates a case of bilateral renal artery stenoses and distal aortic occlusion. The accurate bolus timing and lack of venous overlap enabled easy delineation of the aortic and renal abnormalities. The x-ray angiogram of this patient is shown in Figure 4c. In another patient (Fig 5), the 3D nature of the data set, with high z-resolution (1.5 mm in the anteroposterior direction), clearly demonstrated a left renal artery stenosis in both the coronal and axial projections. Finally, Figure 6 illustrates a complex case in which the patient had multiple abdominal vascular grafts as a result of Takayasu arteritis. The initial examination was performed without fluoroscopic triggering, using instead a fixed delay and sequential phase encoding for the 3D sequence. The resultant image in Figure 6b demonstrates extensive venous overlap obscuring the arterial anatomic structures. A follow-up MR angiogram obtained 6 months later with use of fluoroscopic triggering and elliptical centric phase-encoding order clearly shows all grafts, with no venous overlap (Fig 6c).

In all 25 cases, by using the interactive capability of the fluoroscopic system, it was possible to rapidly obtain a sagittal view of the aorta for monitoring the bolus. In 24 of the 25 fluoroscopically triggered cases, it was possible to trigger the 3D MR angiographic

sequence on the basis of visualization of arrival of contrast material into this imaging plane. The single failure was that of miscommunication, as mentioned earlier. A typical set of fluoroscopic image frames showing arrival of contrast material into the sagittal imaging plane is shown in Figure 7.

Results from the retrospective quantitative analysis of the fluoroscopic frames are shown in Figure 8. In Figure 8a, the transit times from injection to aortic enhancement are plotted against the enhancement factor (postcontrast maximum intensity divided by precontrast intensity from the fluoroscopic images). For the 24 patients, the average time from injection to enhancement of the aorta at the renal arteries was 15.3 seconds ± 4.0 (mean ± standard deviation) and the range of transit times was 8–25 seconds. In Figure 8b, examples of the complete time course from injection to enhancement are shown. In each case, the 3D MR angiographic sequence was triggered at the last point. A decrease in intensity of the last point was common due to inhalation by the patient. In general, the measured degree of contrast material enhancement in the aorta was far less on the fluoroscopic images than on the 3D images. There are three main reasons for this difference: First, the fluoroscopic images were obtained with use of a lower flip angle and longer TR

and thus were subject to increased time-of-flight enhancement; second, the fluoroscopic image sections were typically 10 times thicker than the 3D partitions, and thus the region-of-interest measurements were more influenced by neighboring tissue; and third, the fluoroscopic technique depicted the leading edge of the bolus before maximal enhancement, which ideally would occur by the start of the 3D acquisition a few seconds later.

DISCUSSION

High-quality 3D contrast-enhanced MR angiograms have been demonstrated by many groups without the use of a timing image or direct monitoring. A common approach is to use continuous infusion over the course of the imaging time, with sequential phase-encoding order. The injection is begun such that contrast material will appear in the vessels of interest at the start of imaging. If the timing is accurate, the contrast material will therefore be in the vessels of interest for approximately one-half of the acquisition time before the most central k-space views are acquired. In this time period, the contrast material is likely to migrate into the venous system, and enhancement of the renal vein and vena cava is likely to occur. Reduction of this venous signal intensity can be
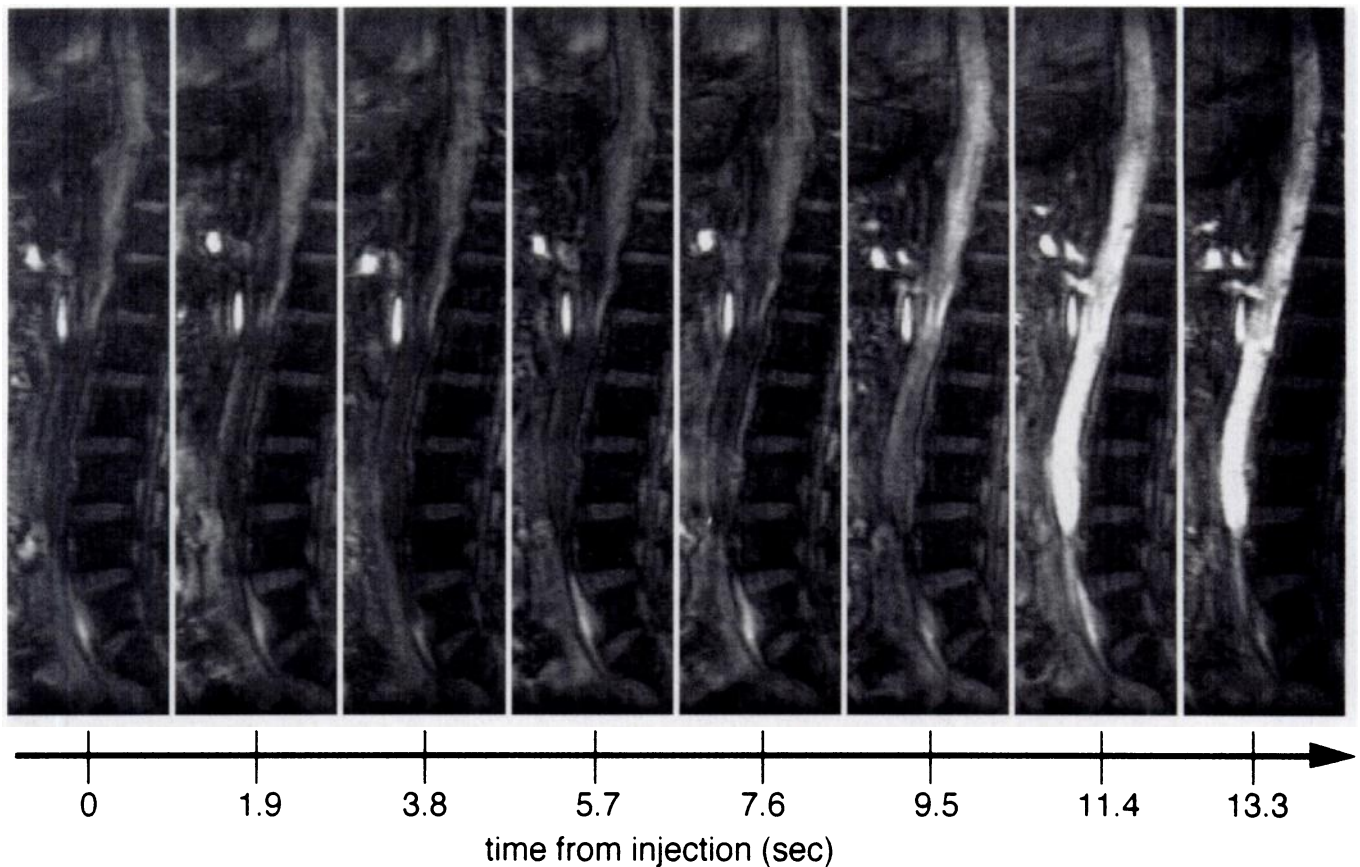
Figure 7. Fluoroscopic images show the arrival of contrast material into the sagittal imaging plane. Only part of each fluoroscopic image is shown, beginning at the time of injection and continuing until when the 3D sequence was triggered. The FOV was 400 mm, and the section thickness was 15 mm. In this case, the TR was 15 msec and a full number of excitations was used, leading to an image update rate of 1.9 seconds.

achieved by using centric ordering; however, the timing of the contrast enhancement then becomes crucial since poor timing can lead to lack of enhancement during the central k-space acquisition. By making use of direct monitoring of the contrast material, consistently accurate timing is possible. When accurate timing is possible, centric encoding may be used and the benefits of improved venous signal suppression and breathing artifact minimization can be reaped.

Recently, venous-suppressed 3D MR angiograms have been obtained by using an initial bolus timing acquisition, followed by a 3D acquisition with sequential order in which the rapid injection is timed such that peak enhancement matches the playout of the central k-space views (16,29). The 3D acquisition is thus similar to Figure 1 part *d*. Although this approach can produce low venous enhancement, it also sacrifices a portion of the high k-space views since many of the initial views are acquired without any contrast material present in the targeted vasculature. The elliptical centric approach also captures the central views at peak arterial enhancement,

but these views are captured in a reduced time period as shown in Figure 1. All of the high k-space views are sampled last when the contrast material is still present in the vasculature. Toward the end of the acquisition, venous enhancement will occur, but the effects are minimized since only high k-space views remain to be sampled.

With regard to bolus timing, the test bolus injection has been shown to provide reliable timing. In a study by Earls et al (16), the average additional time for the performance and evaluation of the timing acquisition was 4.5 minutes. With the fluoroscopic approach, the only additional time is that needed for fluoroscopic localization of the monitoring plane, which was less than 1 minute. Since the fluoroscopic method does not use a test dose, no additional kidney or venous enhancement is introduced. Perhaps most important, the fluoroscopic technique monitors the actual arrival of the contrast material for the 3D MR angiographic acquisition. By using direct monitoring of this dose rather than prediction from an acquisition performed a number of minutes earlier, this technique is unaffected by changes in patient

heart rate or changes in dose delivery rate (possible with manual injection). Immunity to these variables can only aid in increasing the reliability of the technique.

Direct monitoring of contrast material has already been used in 3D MR angiography (18,30). In that approach, a line image through the aorta was used. While that method can provide accurate timing, it does not provide the scope of information available from a 2D image. The typically sagittal image acquisition used in the present work provides an extended view of the aorta from the heart to the lower abdomen, and because of the high spatial resolution, the origins of the major branching vessels (eg, mesenteric and celiac arteries) are typically well seen. The resultant 2D images allow for retrospective analysis of the dynamics of arrival of contrast material at any point on the image. The fluoroscopic triggering approach also differs from that of Foo et al (18) in that the 3D acquisition is triggered by the operator on the basis of specific enhancement of the vessels of interest, as opposed to an automatic trigger arising from a line of data. An auto-
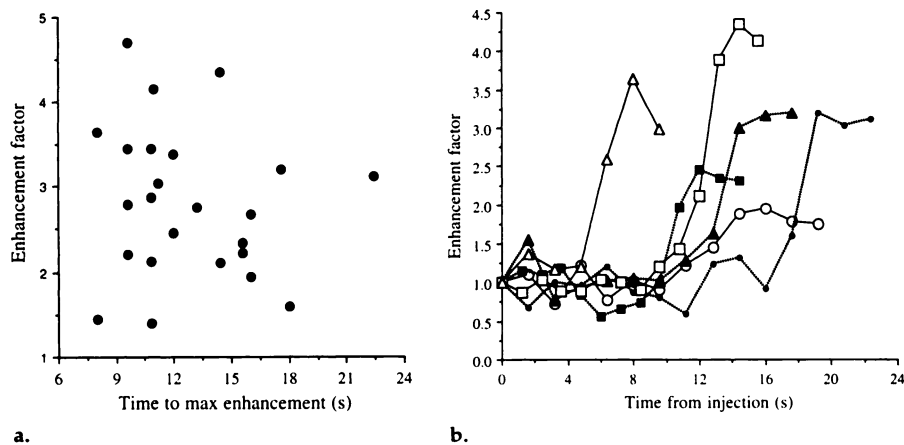
Figure 8. (a) Graph of the enhancement factor of the abdominal aorta plotted against the time to maximum enhancement as determined from the fluoroscopic images in 24 patients. The fluoroscopic enhancement factor was defined as the ratio of aortic signal intensity on the 2D image obtained just before 3D triggering to the signal intensity on the image obtained just before injection. One patient was excluded due to premature triggering of the fluoroscopically triggered sequence. (b) Specific examples of the time course of arrival of contrast material before 3D triggering are shown for six patients. A decrease in signal intensity of the last point was common due to inhalation by the patient after the breath-hold command.

matic triggering method requires the establishment of a specific trigger threshold of signal enhancement; however, Figure 8a illustrates the varying degrees of enhancement. In addition, manual triggering by an experienced operator eliminates the possibility of false triggering arising from respiratory motion, increased blood inflow, gross patient movement, or unusual enhancement problems (4,8,11,15).

At present, the fluoroscopic imaging approach has a slower updating rate than the line scanning approach, which produces an output point every 400 msec (18). Certainly, the fluoroscopic image update rate could be increased to match this rate by sacrificing spatial resolution, by using a higher bandwidth and shorter TRs, or by using partial k-space updating (3,31). In fact, a 64 × 64 resolution would probably be sufficient for bolus detection; however, the detailed depiction of vessel anatomic features provided here would be lost. Further research into the ideal trade-off between spatial resolution and image sampling is necessary.

Time-resolved 3D MR angiography (17) can also consistently produce first-pass arterial images. To achieve this, the k-space data from the 3D volume are sampled repetitively during the breath hold. To allow for a high degree of repetitive sampling within a given time, this technique must limit either the FOV coverage or the spatial resolution. The elliptical centric approach presented here maximizes 3D spatial resolution by sampling each k-space point only once and is con-

strained only by the duration of the breath hold and the length of the bolus.

The elliptical centric encoding scheme has been shown elsewhere to provide superior immunity to breathing artifact (often occurring late in the breath hold) and venous background signal intensity in comparison to many other phase-encoding orders (20,21), including approaches that are based on the centric order used for 2D imaging (32). It is interesting to note, however, that in the present study there was only minor improvement and no statistically significant difference in the degree of motion artifact when using the elliptical centric approach instead of the nontriggered image with sequential phase-encoding order even though the average breath-hold lengths were roughly the same (fluoroscopically triggered, 29 seconds ± 4; nontriggered, 25 seconds ± 5). Although initially surprising, we believe that there are two main reasons as to why the superior motion artifact immunity of the elliptical centric approach was not evident in this study. First, the nontriggered, sequential encoding group benefitted from hyperventilation before the start of the 3D acquisition, whereas in the fluoroscopically triggered cases patients breathed quietly until they were told to quickly hold their breath. Second, the fluoroscopic image operator triggered the 3D acquisition immediately after hearing the "hold your breath" command, and it is conceivable that a number of the patients had not fully held their breath at the triggering time. Since the most central views were acquired first, it was important that the patient had

stopped moving before triggering the 3D acquisition. Typically, the total time between bolus detection at the thoracic aorta and the 3D triggering was under 5 seconds. During this delay, the bolus progressed distally through the abdominal aorta and into the renal artery tree.

The venous-suppressed MR angiograms shown in this work arise from the combined use of fluoroscopic triggering and an elliptical centric phase-encoding order. Both innovations are important. If one were to perform elliptical centric phase encoding without an accurate bolus timing scheme, it is unlikely that the central views would be acquired at peak arterial enhancement, and this could lead to substantial artifacts (4). Alternatively, if one were to perform fluoroscopic triggering with a sequential phase-encoding order, the bolus would peak long before the central views were acquired (Fig 1 part c) resulting in substantial venous enhancement. Hence, the fluoroscopic triggering approach requires the use of a centric phase-encoding order. Our choice of the elliptical centric order was based on the extensive evaluation of centric phase-encoding orders (21). In particular, when the bolus is properly timed, this technique has been shown to limit venous enhancement more effectively than other commonly used 3D centric approaches because the central views are sampled first in the most compact period possible.

The equipment described here for performing the fluoroscopic acquisition and triggering of the 3D acquisition is not presently widely available. Although this equipment was custom developed in our own laboratory, many of the elements are already intrinsic to most commercial MR imaging systems. In fact, the most expensive element of the hardware used here was the array processor, and such a device is already found in virtually all current commercial systems. Implementation of this technique on commercial systems would principally require that the data flow, image reconstruction, and sequence switching be performed faster than is typically done currently.

In addition to cost, another practical aspect of any new technology is the expertise required to operate it. In the initial phases of this project, the equipment was operated by the senior author (A.H.W.). However, as the procedures for fluoroscopic positioning and setup of the 3D MR angiographic acquisition became more standardized, equipment operation for many of the patient studies was done by a techni-

cian. We fully expect that MR technologists will be readily capable of operating the fluoroscopic equipment.

In conclusion, fluoroscopic 2D imaging provides a reliable method for timing the arrival of the bolus of contrast material to the specific area of interest. When combined with a 3D MR angiographic acquisition with use of an elliptical centric view order, it is possible to consistently obtain high-quality, high-resolution, arterial-phase, relatively motion immune angiograms. ■

References

1. Prince MR, Yucel EK, Kaufman JA, Harrison DC, Geller SC. Dynamic gadolinium-enhanced 3D abdominal MR arteriography. JMRI 1993; 3:877–881.
2. Prince MR. Gadolinium-enhanced MR aortography. Radiology 1994; 191:155–164.
3. Riederer SJ, Tasciyan T, Farzaneh F, Lee JN, Wright RC, Herfkens RJ. MR fluoroscopy: technical feasibility. Magn Reson Med 1988; 8:1–15.
4. Maki JH, Prince MR, Londy FJ, Chenevert TL. The effects of time varying intravascular signal intensity and k-space acquisition order on three-dimensional MR angiography image quality. JMRI 1996; 6:642–651.
5. Adamis MK, Li W, Wielopolski PA, et al. Dynamic contrast-enhanced subtraction MR angiography of the lower extremities: initial evaluation with a multisection two-dimensional time-of-flight sequence. Radiology 1995; 196:689–695.
6. Wang Y, Johnston DL, Breen JF, et al. Dynamic MR digital subtraction angiography using contrast enhancement, fast data acquisition, and complex subtraction. Magn Reson Med 1996; 36:551–556.
7. Hennig J, Scheffler K, Laubenberger J, Strecker R. Time-resolved projection angiography after bolus injection of contrast agent. Magn Reson Med 1997; 37:341–345.
8. Holland GA, Dougherty L, Carpenter JP, et al. Breath-hold ultrafast three-dimensional gadolinium-enhanced MR angiography of the aorta and the renal and other visceral abdominal arteries. AJR 1996; 166: 971–981.
9. Earls JP, Rofsky NM, DeCorato DR, Krinsky GA, Weinreb JC. Hepatic arterial-phase dynamic gadolinium-enhanced MR imaging: optimization with a test examination and a power injector. Radiology 1997; 202:268–273.
10. Creasy JL, Price RR, Presbrey T, Goins D, Partain CL, Kessler RM. Gadolinium-enhanced MR angiography. Radiology 1990; 175:280–283.
11. Prince MR, Narasimham DL, Stanley JC, et al. Breath-hold gadolinium-enhanced MR angiography of the abdominal aorta and its major branches. Radiology 1995; 197:785–792.
12. Shetty AN, Shirkhoda A, Bis KG, Alcantara A. Contrast-enhanced three dimensional MR angiography in a single breath-hold: a novel technique. AJR 1995; 165:1290–1292.
13. Isoda H, Ushimi T, Masui T, et al. Clinical evaluation of pulmonary 3D time-of-flight MRA with breath holding using contrast media. J Comput Assist Tomogr 1995; 19: 911–919.
14. Leung DL, McKinnon GC, Davis CP, Pfammatter T, Krestin GP, Debatin JF. Breath-hold, contrast-enhanced, three-dimensional MR angiography. Radiology 1996; 201:569–571.
15. Steiner P, McKinnon GC, Romanowski B, Goehde SC, Hany T, Debatin J. Contrast-enhanced, ultrafast 3D pulmonary MR angiography in a single breathhold: initial assessment of imaging performance. JMRI 1997; 7:177–182.
16. Earls JP, Rofsky NM, DeCorato DR, Krinsky GA, Weinreb JC. Breath-hold single-dose gadolinium-enhanced three-dimensional MR aortography: usefulness of a timing examination and MR power injector. Radiology 1996; 201:705–710.
17. Korosec FR, Frayne R, Grist TM, Mistretta CA. Time-resolved contrast-enhanced 3D MR angiography. Magn Reson Med 1996; 36:345–351.
18. Foo TKF, Saranathan M, Prince MR, Chenevert TL. Automated detection of bolus arrival and initiation of data acquisition in fast, three-dimensional, gadolinium-enhanced MR angiography. Radiology 1997; 203:275–280.
19. Wilman AH, Riederer SJ, Breen J, Ehman RL. Elliptical spiral phase encode ordering: a dynamic, field-of-view–dependent scheme for breath-hold contrast-enhanced MR angiography (abstr). Radiology 1996; 201(P):328.
20. Wilman AH, Riederer SJ. An optimal phase encoding order for minimizing motion and maximizing arterial contrast in 3D contrast-enhanced MR angiography (abstr). Proceedings of the Fifth Meeting of the International Society for Magnetic Resonance in Medicine. Berkeley, Calif: International Society for Magnetic Resonance in Medicine, 1997; 252.
21. Wilman AH, Riederer SJ. Performance of an elliptical spiral centric view order for signal enhancement and motion artifact suppression in breathhold three dimensional gradient echo imaging. Magn Reson Med (in press).
22. Wilman AH, Riederer SJ. Improved centric phase encoding orders for three dimensional magnetization prepared MR angiography. Magn Reson Med 1996; 36:384–392.
23. Hangiandreou NJ, Debbins JP, Rossman PJ, Riederer SJ. Interactive selection of optimal section orientations using real-time MRI. Magn Reson Med 1995; 34:114–119.
24. Hayes CE, Hattes N, Roemer PB. Volume imaging with MR phased arrays. Magn Reson Med 1991; 18:309–319.
25. Wright RC, Riederer SJ, Farzaneh F, Rossman PJ, Liu Y. Real-time MR fluoroscopic data acquisition and image reconstruction. Magn Reson Med 1989; 12:407–415.
26. Debbins JP, Riederer SJ, Rossman PJ, et al. Cardiac magnetic resonance fluoroscopy. Magn Reson Med 1996; 36:588–595.
27. Campeau N, Johnson C, Felmlee J, et al. MR imaging of the abdomen with a phased array multicoil: prospective clinical evaluation. Radiology 1995; 195:769–776.
28. Rosner B. Fundamentals of biostatistics. 3rd ed. Boston, Mass: Duxbury, 1990; 304–307.
29. Hany TF, McKinnon GC, Leung DA, Pfammatter T, Debatin JF. Optimization of contrast timing for breath-hold three-dimensional MR angiography. JMRI 1997; 7:551–556.
30. Prince MR, Chenevert TL, Foo TK, Londy FJ, Ward JS, Maki JH. Contrast-enhanced abdominal MR angiography: optimization of imaging delay time by automating the detection of contrast material arrival in the aorta. Radiology 1997; 203:109–114.
31. van Vaals JJ, Brummer ME, Dixon WT, et al. "Keyhole" method for accelerating imaging of contrast agent uptake. JMRI 1993; 3:671–675.
32. Bampton AEH, Riederer SJ, Korin HW. Centric phase encoding order for 3D magnetization-prepared gradient echo sequences: application to abdominal imaging. JMRI 1992; 2:327–334.